The Electronic Conductivity of Single Crystalline Ga-Stabilized Cubic Li$_7$La$_3$Zr$_2$O$_{12}$: A Technologically Relevant Parameter for All-Solid-State Batteries

Martin Philipp, Bernhard Gadermaier, Patrick Posch, Ilie Hanzu, Steffen Ganschow, Martin Meven, Daniel Rettenwander, Günther J. Redhammer, and H. Martin R. Wilkening*

The next-generation of all-solid-state lithium batteries need ceramic electrolytes with very high ionic conductivities. At the same time a negligible electronic conductivity σ_{eon} is required to eliminate self-discharge in such systems. A non-negligible electronic conductivity may also promote the unintentional formation of Li dendrites, being currently one of the key issues hindering the development of long-lasting all-solid-state batteries. This interplay is suggested recently for garnet-type Li$_7$La$_3$Zr$_2$O$_{12}$ (LLZO). It is, however, well known that the overall macroscopic electronic conductivity may be governed by a range of extrinsic factors such as impurities, chemical inhomogeneities, grain boundaries, morphology, and size effects. Here, advantage of Czochralski-grown single crystals, which offer the unique opportunity to evaluate intrinsic properties of a chemically homogeneous matrix, is taken to measure the electronic conductivity σ_{eon}. Via long-time, high-precision potentiostatic polarization experiments an upper limit of σ_{eon} in the order of 5×10^{-10} S cm^{-1} (293 K) is estimated. This value is by six orders of magnitude lower than the corresponding total conductivity $\sigma_{total} = 10^{-3}$ S cm^{-1} of Ga-LLZO. Thus, it is concluded that the high values of σ_{eon} recently reported for similar systems do not necessarily mirror intragrain bulk properties of chemically homogenous systems but may originate from chemically inhomogeneous interfacial areas.

1. Introduction

Cutting our dependency on fossil fuels requires powerful systems that can efficiently store electricity from so-called renewable but intermittent energy sources such as solar, wind or tidal.[1] Lithium-ion batteries with insertion hosts[2] are currently the most powerful electrochemical storage systems used in portable electronics and in the transportation sector.[2c,3] To increase both their energy and power density, the use of Li metal as anode material is re-envisaged since a couple of years.[4] The replacement of flammable liquid electrolytes used in conventional systems by ceramic ones is expected to enable the safe use of Li metal and to widen the thermal stability window of such systems. For practical reasons, the ionic conductivity σ_{ion} of suitable ceramic electrolytes, acting as electronic insulators, should, however, be in the order of 1 mS cm^{-1} or higher to ensure proper battery operation at ambient and lower temperatures. The garnet-type solid electrolyte Li$_7$La$_3$Zr$_2$O$_{12}$ (LLZO)[5] crystallizing with cubic symmetry definitely represent one of the frontrunners in the group of the most promising oxidic solid electrolytes.[6] With their outstanding ionic conductivity,[7] and their wide electrochemical stability window, they are envisaged to play an important role in both the development of volume-type[8] and thin-film batteries.[9] Of course, sulfide-based electrolytes or thiophosphates show even

M. Philipp, B. Gadermaier, Dr. P. Posch, Dr. I. Hanzu,
Dr. D. Rettenwander, Prof. H. M. R. Wilkening
Institute for Chemistry and Technology of Materials, Christian Doppler
Laboratory for Lithium Batteries
Graz University of Technology (NAWI Graz)
Stremayrgasse 9, Graz 8010, Austria
E-mail: wilkening@tugraz.at
Dr. I. Hanzu, Prof. H. M. R. Wilkening
Alistore-ERI European Research Institute
CNRS FR3104
Hub de l'Energie, Rue Baudelocque, Amiens 80039, France

Dr. S. Ganschow
Leibniz-Institut für Kristallzüchtung
Max-Born-Str. 2, Berlin 12489, Germany
Dr. M. Meven
Institute of Crystallography
RWTH Aachen University
Aachen 52056, Germany
Dr. M. Meven
Jülich Centre for Neutron Science (JCNS)
Forschungszentrum Jülich GmbH at Heinz
Maier-Leibnitz Zentrum (MLZ)
Garching 85748, Germany
Prof. G. J. Redhammer
Department of Chemistry and Physics of Materials
Jakob-Haringer-Strasse 2a
University of Salzburg
Salzburg 5020, Austria

higher conductivity values[10] but suffer from their air-sensitivity and electrochemical instability.[11]

To circumvent unwanted self-discharge and the occurrence of internal short circuits evoked by Li dendrites,[12] which is, in general, one of the main safety risks of batteries,[13] the ceramic electrolyte has to exhibit negligible electronic conductivity σ_{eon}. The suppression of Li dendrite formation by suitable interface engineering thus belongs to the key tasks in battery research.[13] Very recently, Han et al. suggested that a very low but non-negligible value of σ_{eon} (10^{-8} S cm^{-1}) can provoke the formation of Li dendrites in LLZO-type garnets.[14]

Han et al., however, used polycrystalline samples and the same holds for the other very few studies, which appeared in literature so far. In all cases polycrystalline samples were studied that had been stabilized in their cubic modification by supervalent doping. Depending on the exact stoichiometry, including the defect chemistry in the bulk and in surface regions, as well as the measurement conditions σ_{eon} values presented in literature differ, however, by more than four orders of magnitude.[14,15] This finding shows that the influence of (local) chemical inhomogeneities, surface morphologies and particularly that of the grain boundaries regions[12] on σ_{eon} is still not clear. One might expect that these regions in LLZO show slightly different compositions and defect structures as compared to the situation in the grains. Thus, surface areas and grain boundary (g. b.) regions, inevitably forming a percolating network in any pelletized sample, could show a higher electronic conductivity than that present in the crystalline grains, as also suggested by Tian et al.[16] In other words, these regions, as also seen in other ceramics,[17] might act as fast pathways for electrons or polarons causing the relatively high electronic conductivities seen in some of the samples studied so far.[12] Such extrinsic, interfacial effects will, however, mask intragrain properties.

Here, we took advantage of chemically homogeneous Czochralski-grown LLZO-type crystals of the nominal composition Li$_{6.4}$Ga$_{0.2}$La$_3$Zr$_2$O$_{12}$ to study both bulk electronic conductivities σ_{eon} and total conductivities σ_{total}. The acentric crystal structure of Ga-LLZO is shown in **Figure 1**. While the general structure of the cubic garnet is depicted in Figure 1a, highlighting the densely packed structure, the complex distribution of Li ions among three different crystallographic sites is presented in Figure 1b. Jumping between these sites enables the Li ions to move easily over long distances. The structure has in detail been described by Wagner et al.,[18] see also the Supporting Information for further structural details.

Having single crystals at hand, we used high-precision potentiostatic polarization measurements to reveal the upper limit of σ_{eon} that refers to the intragrain regions in cubic Ga-stabilized LLZO. As yet, only few studies[14,15] focused, however, on the estimation or measurement of the electronic conductivity that contributes to the total conductivity in LLZO. In general, a clear separation of ionic and electronic contributions is by far not trivial[19] and has been documented for few other materials.[20]

2. Results and Discussion

LLZO, if present in its tetragonal modification (space group $I4_1/acd$), exhibits a low ionic conductivity of $\approx 10^{-6}$ S cm^{-1} at room temperature.[21] Upon heating, the crystal structure changes to a cubic modification ($Ia\bar{3}d$) and the ionic conductivity increases by almost three orders of magnitude.[22] Using supervalent dopants such as Ga, Ta or Al, cubic, or in the case of Ga, acentric modifications, crystallizing with the space group $I\bar{4}3d$, can be stabilized at much lower temperatures. These samples yield, in the ideal case, room-temperature (total) conductivities reaching values of 1 mS cm^{-1} or conductivities (slightly) above this value;[23] as an example Qin et al. reached 2 mS cm^{-1} if Ga-LLZO is present in a self-textured form.[24] Here, we studied Czochralski-grown Ga-stabilized LLZO single crystals with total room-temperature conductivities in this order of magnitude, 1 mS cm^{-1} (293 K).

In **Figure 2**a the real part of the complex conductivity σ', measured at 293 K, is plotted as a function of the period, which is the inverse of the frequency ν. The corresponding conductivity isotherms are shown in **Figure 3**a. They are composed of three regimes I to III, as also indicated in Figure 3b. At low frequencies a frequency-dependent polarization regime I is seen that passes into the so-called frequency independent direct current (DC) conductivity plateau (regime II). A stepwise decay of σ' in regime I is, most likely, due to the formation of space charge zones in front of the ion-blocking electrode[25] that also slow down ion transport farther away from the electrode. Due to the high total conductivity σ_{DC} ($\equiv \sigma_{total}$), the dispersive regime III, characterized by an increase of σ' at high frequencies according to Jonscher's power law, is only seen at the lowest temperatures (see Figure 3a). The isotherm recorded at 293 K reveals that σ_{DC}, being the total conductivity, turned out to be 1 mS cm^{-1}. At this temperature, σ' steadily decreases if we go to frequencies lower than 10^4 Hz. This strong polarization effect already indicates that σ_{eon} is at least lower than 10^{-7} S cm^{-1}. Note that the electrodes applied are nonblocking for e$^-$; thus, σ_{eon} is expected to show a plateau at sufficiently low ν, i.e., at values being considerably lower than 10^{-2} Hz.

The electronic conductivity of the Ga-LLZO single crystal was probed by using potentiostatic polarization measurements using symmetric Au|Ga-LLZO|Au cells; polarization curves were recorded at various temperatures and potentials. Thereby,
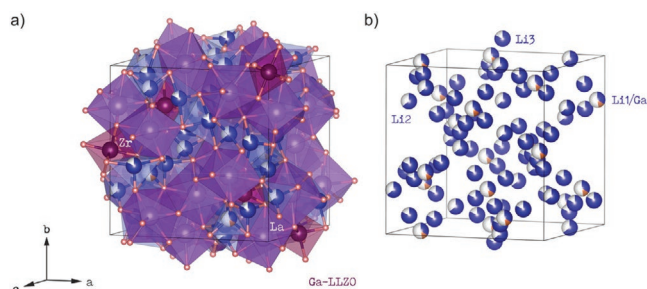

Figure 1. a,b) Crystal structure of Ga-containing Li$_{6.4}$Ga$_{0.2}$La$_3$Zr$_2$O$_{12}$ (space group $I\bar{4}3d$ (No. 220)) as determined by a combined, simultaneous refinement of both data from X-ray diffraction and neutron diffraction, see Tables S1 and S2 of the Supporting Information for further details. The Li ions are distributed over three different crystallographic sites (12a (Li1), 12b (Li2), 48e (Li3)) in the acentric space group. Ga^{3+} ions share sites with Li$^+$ located at the Li1 site, being the Wyckoff position 12a. The Li$^+$ ions form a 3D network enabling them to quickly diffuse through the crystal structure.

**ADVANCED
SCIENCE NEWS**

www.advancedsciencenews.com

**ADVANCED
MATERIALS
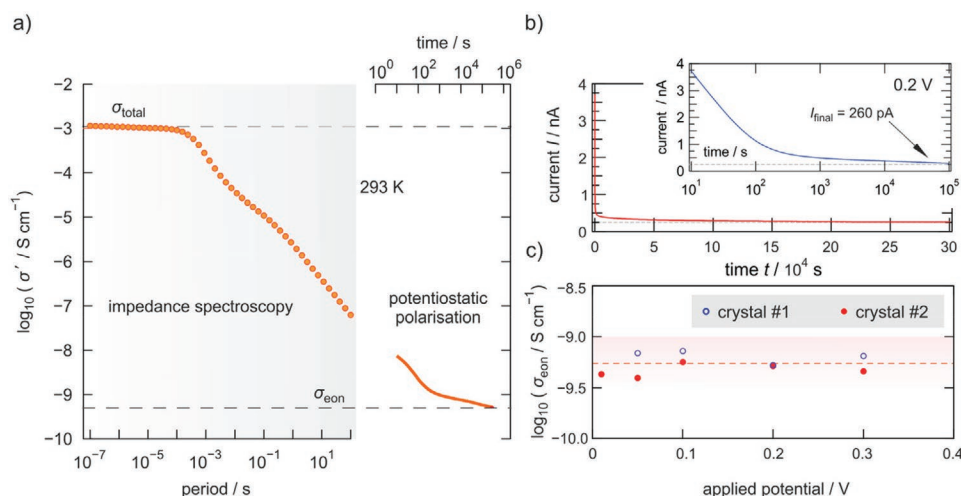INTERFACES**

www.advmatinterfaces.de

Figure 2. a) Conductivity isotherm of a Ga-stabilized LLZO single crystal as obtained by broadband impedance spectroscopy using ion-blocking Au electrodes. σ' is shown as a function of the period, being the inverse frequency. On the right hand side of the result of our potentiostatic (0.2 V) polarization measurement is shown. It already indicates that σ' will reach a plateau pointing to an electronic conductivity lower than 10^{-9} S cm^{-1}. b) Evolution of the current I with increasing time during potentiostatic polarization at 0.2 V and 293 K. The residual current is expected to be purely electronic (same data as shown in (a)). The inset shows the same curve, however, with the time axis plotted logarithmically. c) Specific electronic conductivity σ_{eon} of two different single crystals with the same composition at potentials ranging from 10 to 300 mV.

we measured the evolution of the current I over an extended time window of up to 3×10^5 s, i.e., for a period of >83 h. At room temperature, we found that the final (or steady-state) current $I_{final} = 260$ pA, which we assume to be electronic in origin, corresponds to σ_{eon} that is at least six orders of magnitude lower than σ_{total} (see also Figure 2b). Specific electronic conductivities, taking the area and thickness of the sample and the applied potential into account, are shown in Figure 2c. The electronic conductivity was measured for two different single crystals and at different potentials ranging from 10 to 300 mV (see Figure 2c). As the values are identical within a factor of 2, we assume that the potential applied was chosen to be well below the decomposition potential for Ga-LLZO.[26]

In Figure 3b the total conductivity of Ga-LLZO is plotted as a function of the inverse temperature $1/T$ in an Arrhenius graph; data were read off from the isotherms shown in Figure 3a, see above. Considering the negligible electronic contribution to the total conductivity, which amounts in our case to be less than 1 ppm, we can safely assume that $\sigma_{ion} = \sigma_{total}$ and, thus, expect a classical Arrhenius relation between σ and $1/T$. Analyzing our data according to $\sigma T = \sigma_0 \exp(-E_a/(k_B T))$ we obtain an activation energy E_a of 0.30(1) eV (see Figure 3a); σ_0 denotes the pre-exponential factor and k_B is Boltzmann's constant. Such a low activation energy is a typical value for fast ion conductors and has been found for a row of solid electrolytes such as Li-bearing argyrodites,[27] NaSICON-type electrolytes,[28] and
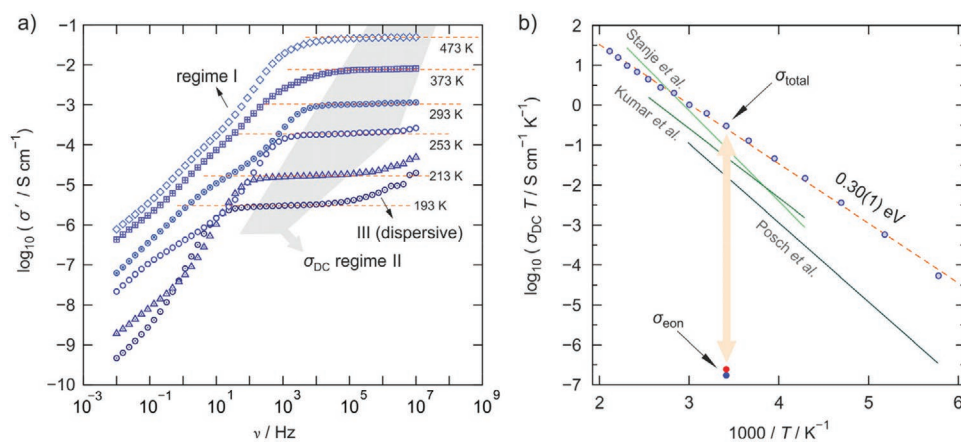

Figure 3. a) Conductivity isotherms of a Ga-LLZO single crystal showing the real part of the complex conductivity versus the applied frequencies. Temperatures are indicated; the isotherms are composed of three regimes labeled I, II, and III, see text for further explanation. The broad frequency-independent DC plateau (regime II) is followed by electrode polarization effects appearing at lower frequencies. Only at very low temperatures T the Jonscher-type dispersive regime III is accessible in the frequency range used to record the isotherms. b) Arrhenius plot of the total conductivity σ_{total} read off from regime II yielding an activation energy as low as 0.3 eV. The mean electronic conductivity σ_{eon} of two single crystals investigated at room temperature is also shown. For comparison, the total conductivity for Al-stabilized single crystalline LLZO (Posch et al.[32a]), Ta-stabilized single crystalline LLZO (Stanje et al.[22]), and Al-stabilized polycrystalline LLZO (Kumar et al.[32b]) are included as well.
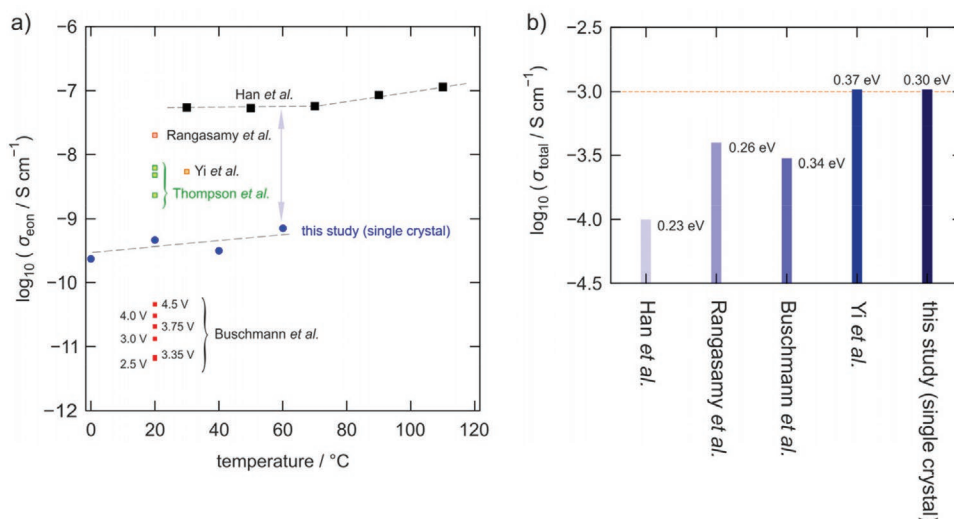
**ADVANCED
SCIENCE NEWS**
www.advancedsciencenews.com

**ADVANCED
MATERIALS
INTERFACES**
www.advmatinterfaces.de

Figure 4. a) Change of the electronic conductivity of single crystalline Ga-LLZO as measured in this study as a function of temperature. For comparison, σ_{eon} values of other studies of cubic LLZO stabilized by the incorporation of either Al^{3+}, Ta^{3+}, or Ga^{3+} ions are also included; of course, these studies focus on charge carrier transport in LLZO-type garnets with different compositions. b) Total conductivities σ_{total} (and corresponding activation energies) that refer to the results on polycrystalline samples shown in (a).

the Ti- and Ge-containing thiophosphates such as lithium titanium phosphate[29] and lithium germanium thiophosphate.[30] Importantly, the value is well in line with that obtained from total conductivity measurements in highly dense polycrystalline Ga-LLZO samples with negligible g. b. contributions.[31] For comparison, in Figure 3b results from other LLZO samples are included as well.[22,32]

The temperature dependence of σ_{eon} is shown in **Figure 4**a. It revealed a weak thermal activation pointing to an activation energy of 0.14(7) eV. For comparison, the values of Han et al.[14] yield an activation energy of 0.23(2) eV for polycrystalline $Li_{6.4}La_3Zr_{1.4}Ta_{0.6}O_{12}$. Note, however, that the polarization time in their study was only 1 h at 100 mV (200 nm thick Cu electrodes). Values of their study are included in Figure 4a; compared to this work σ_{eon} is higher by two orders of magnitude and might play a role in Li dendrite formation as assumed by the authors. Rangasamy et al.[15b] investigated the ionic and electronic conductivity of Al-doped polycrystalline garnets with the composition $Li_{6.24}Al_{0.24}La_3Zr_2O_{11.98}$; they found $\sigma_{total} = 4 \times 10^{-4}$ S cm^{-1} with an activation energy of $E_a = 0.26$ eV and an electronic conductivity σ_{eon} of 2×10^{-8} S cm^{-1} at room temperature. Again, this value is by approximately two orders of magnitude higher than that probed in this study. A very similar value of 3.59×10^{-8} S cm^{-1} has been reported by Song et al. for polycrystalline $Li_7La_{2.75}Ca_{0.25}Zr_{1.75}Nb_{0.25}O_{12}$;[12] the authors point out the importance of grain boundary regions to be responsible for enhanced electronic conduction.[16,17] As has been shown in the elegant study of Song et al.[26] the electronic conductivity in polycrystalline LLZO samples, if high potentials are applied, is best described by the behavior of a varistor, exhibiting a potential-dependent electronic resistance. If the applied electric voltage exceeds a certain limit, electric breakdown at the grain boundaries will occur and significantly increase the electronic conductivity; below this threshold, LLZO shows ohmic behavior. Obviously, the electric field the grain boundaries can

withstand depends on the local composition including, for example, impurities, segregated phases, and vacancies. A general discussion of this effect and the influence of even small variations of the dopant concentration is given in Zhao et al.[33]

In an earlier work Buschmann et al.[15a] presented a total conductivity of 3×10^{-4} S cm^{-1} for Al-stabilized (0.9% wt) polycrystalline garnets, which is very similar to that of Rangasamy et al.[15b] The corresponding activation energy turned out to be 0.34 eV.[15a] The specific electronic conductivity was measured by the Hebb–Wagner technique at potentials ranging from 2.5 to 4.5 V; very low values of 6.4×10^{-12} S cm^{-1} (2.5 V) and 4.6×10^{-11} S cm^{-1} (4.5 V) were reported. Yi et al.[15d] investigated the ionic and electronic conductivity of polycrystalline Al-free but Ta-stabilized LLZO ($Li_{6.7}La_3Zr_{1.7}Ta_{0.3}O_{12}$). By using Ag electrodes and a constant potential of 100 mV they found that the specific electronic conductivity σ_{eon} takes values in the order of 5.4×10^{-9} S cm^{-1}. This value was obtained after 8 min of polarization; for comparison, the total conductivity was 10^{-3} S cm^{-1} at 303 K (0.37 eV). Thompson et al.[15c] studied the electronic conductivity of Ta-bearing as well as Al-stabilized polycrystalline cubic LLZO samples in a semiblocking cell configuration (Li|LLZO|Au) at various potentials. The corresponding values are also included in Figure 4a. Figure 4b summarizes the total conductivities at room temperature that refer to the results for the samples included in Figure 4a.

We notice that even for similar polycrystalline samples the specific electronic conductivity may differ by some orders of magnitude. Although different methods have been employed to measure σ_{eon}, we can group the data that has been derived by applying low potentials. In this group, the electronic conductivity measured in Ga-LLZO single crystals turns out to be the lowest one and cannot be affected by any g. b. contributions,[26] thus representing a pure bulk value. This observation is in line with the general finding that the electronic conductivity of garnets is higher in polycrystalline than in single crystalline samples.[34]

Single crystalline Ga-LLZO studied here has to be characterized by a relatively high ionic conductivity, its electronic conductivity, on the other hand, turned out to be rather low.[35] Hence, also by considering results in literature presented so far, it is very likely that electron transport is not coupled with ion transport, as it may happen in some other materials with poor ion conducting properties.[36] The low activation energy associated with electronic conductivity is very likely the key reason for this decoupling. Having a low activation energy, the electron mobility is significantly less influenced by the temperature than the ionic mobility. While electrons are mobile at all times, the concentration of electron defects is most likely extremely low, thus accounting for the low electronic conductivity seen in polarization experiments.

We should consider the value for σ_{eon} as an upper limit for the electronic conductivity. We assume that the sandwich pellet equipped with the two ion-blocking electrodes reaches a stationary state after a certain time under polarization. This state should be seen as a dynamic equilibrium in which the flux of ions moving from or toward the interfaces under the applied electric field equals the flux of ions that move in the opposite direction due to the formation of ion concentration gradients. We anticipate that in addition to the flux of Li$^+$ ions, oxygen ion transport[37] is by several orders of magnitude lower than that associated with I_{final}. Also, it is assumed that local electric fields and those forming in front of the metal electrodes (the induced space charge fields) are negligible and do not lead to any breakdown phenomena and/or electrochemical reaction. This assumption also includes that no leakage currents contribute to the steady-state values obtained after a sufficiently long period of polarization. In our opinion, taking into account such effects, which are extremely hard to quantify separately, would yield even lower values for σ_{eon}. Nevertheless, the value of the electronic part of conductivity determined by the simple polarization method used here, while certainly affected by some errors, represents a technologically relevant parameter. In a real solid-state battery, the electrodes will always be good electron conductors and the solid electrolyte will continuously face a certain polarization voltage, depending on the operational potential of the electrodes and state of charge. Thus, for any practical application, it would be important to know what is the apparent electronic conductivity to estimate the self-discharge current caused by i) overall electron transport through the solid electrolyte and by ii) electron transport through the crystal lattice.

3. Conclusion

Here, we probed the electronic and ionic conductivity of single crystalline, Czochralski-grown Ga-stabilized Li$_{6.4}$Ga$_{0.2}$La$_3$Zr$_2$O$_{12}$ by means of broadband impedance spectroscopy and potentiostatic polarization. To stay well below the decomposition potential of LLZO we chose very low potentials to polarize a symmetric Au|Ga-LLZO|Au cell. We found that the electronic conductivity, as estimated from polarization curves, is at least six orders of magnitude lower than the total conductivity to which impedance spectroscopy is, at sufficiently high frequencies, sensitive. In contrast to earlier speculations we think that in the present case a residual electric conductivity in the order of 10^{-10} S cm^{-1} does not trigger the formation of Li dendrites.

In the present case, Li$^+$ transport in Ga-LLZO turned out to be independent and, thus, not coupled with the residual electronic bulk conductivity.

4. Experimental Section

Single crystals with the composition Li$_{6.4}$Ga$_{0.2}$La$_3$Zr$_2$O$_{12}$ were directly grown from the melt by the Czochralski method. The advantages of this method over many other methods of producing crystalline materials are that it yields large single crystals. Furthermore, the elemental distribution of dopants in a single crystal is homogeneous compared to polycrystalline samples.[38] In the context of this study, the advantage lies foremost in the fact that a large single crystal could be produced. The starting materials Li$_2$CO$_3$ (Alfa Aesar, 99.999%), La$_2$O$_3$ (Fox Chemicals, 99.999%), Ga$_2$O$_3$ (Fox Chemicals, 99.999%), and ZrO$_2$ (Merck, Optipur) were dried and then mixed with an excess of 10 wt% of Li$_2$CO$_3$. The mixture was isostatically pressed and calcined at a maximum temperature of 1230 °C following the procedure commonly used for the preparation of LLZO ceramic samples.[18] Afterward, the material was melted in an inductively heated iridium crucible in N$_2$ atmosphere. Crystallization was initiated by dipping an iridium wire into the supercooled melt; this wire was slowly pulled upward at a constant rate of 0.4 mm h^{-1} under rotation of 10 min^{-1}. After growth, the crystal was cooled down to room temperature within 15 h. The obtained crystal was 14 mm in diameter and about 50 mm long, it is of yellow color with white opaque adhesions and some cracks. However, the interior was mainly transparent and allowed for the preparation of several smaller measurement specimens. The singe crystals were characterized by X-ray diffraction and neutron diffraction (Tables S1 and S2, Supporting Information).

For the measurement of total and electronic conductivity the crystals were cut into square specimens (5 mm) and a thickness of 1 mm. To remove any newly formed surface contaminations, such as thin layers of Li$_2$CO$_3$, they were transferred into an Ar-filled glovebox (H$_2$O and O$_2$ < 1 ppm) and thoroughly polished with sanding paper (SiC, 4000 grit). Then, ion blocking electrodes were applied (100 nm, Au) by means of sputtering, again under inert gas atmosphere. The total conductivity, that is the sum of the ionic and the electronic conductivity, was measured on symmetric Au|Ga-LLZO|Au pellets with a Concept80 broadband impedance spectrometer (Novocontrol) applying a root-mean-square (rms) sinusoidal voltage amplitude of 0.1 V$_{rms}$. Conductivity isotherms were recorded over a broad frequency range (10^{-2} and 10^7 Hz) and at different temperatures ranging from 173 to 373 K. For potentiostatic polarization, the samples in sandwich configuration were kept in an airtight Swagelock-type cell and subjected to a constant potential (Parstat MC potentiostat); the current I was recorded as a function of time t. Polarization measurements using ion-blocking Au electrodes were performed at 273, 293, 313, and at 333 K. The steady state current I_{final} corresponds to the residual electronic current, which can be converted into the specific electronic conductivity σ_{eon}. Here, the well-known Hebb–Wagner method is not used to assess σ_{eon} as LLZO is not thermodynamically stable in contact with metallic lithium.[39]

Supporting Information

Supporting Information is available from the Wiley Online Library or from the author.

Acknowledgements

[1] D. Larcher, J. M. Tarascon, *Nat. Chem.* **2015**, *7*, 19.

[2] a) M. S. Whittingham, *Chem. Rev.* **2014**, *114*, 11414; b) M. S. Whittingham, *Chem. Rev.* **2004**, *104*, 4271; c) J. B. Goodenough, Y. Kim, *Chem. Mater.* **2010**, *22*, 587.

[3] a) M. Li, J. Lu, Z. W. Chen, K. Amine, *Adv. Mater.* **2018**, *30*, e1800561; b) J. W. Choi, D. Aurbach, *Nat. Rev. Mater.* **2016**, *1*, 16013; c) B. Scrosati, J. Hassoun, Y. K. Sun, *Energy Environ. Sci.* **2011**, *4*, 3287.

[4] J. B. Goodenough, *Energy Storage Mater.* **2015**, *1*, 158.

[5] R. Murugan, V. Thangadurai, W. Weppner, *Angew. Chem., Int. Ed.* **2007**, *46*, 7778.

[6] a) X. Huang, Y. Lu, Z. Song, T. Xiu, M. E. Badding, Z. Wen, *J. Energy Chem.* **2019**, *39*, 8; b) F. Flatscher, M. Philipp, S. Ganschow, H. M. R. Wilkening, D. Rettenwander, *J. Mater. Chem. A* **2020**, https://doi.org/10.1039/C9TA14177D.

[7] a) V. Thangadurai, S. Narayanan, D. Pinzaru, *Chem. Soc. Rev.* **2014**, *43*, 4714; b) J. C. Bachman, S. Muy, A. Grimaud, H. H. Chang, N. Pour, S. F. Lux, O. Paschos, F. Maglia, S. Lupart, P. Lamp, L. Giordano, Y. Shao-Horn, *Chem. Rev.* **2016**, *116*, 140; c) A. Manthiram, X. Yu, S. Wang, *Nat. Rev. Mater.* **2017**, *2*, 16103; d) F. Zheng, M. Kotobuki, S. Song, M. O. Lai, L. Lu, *J. Power Sources* **2018**, *389*, 198; e) J. Schnell, T. Günther, T. Knoche, C. Vieider, L. Köhler, A. Just, M. Keller, S. Passerini, G. Reinhart, *J. Power Sources* **2018**, *382*, 160.

[8] S. Afyon, K. V. Kravchyk, S. Wang, J. van den Broek, C. Hänsel, M. V. Kovalenko, J. L. M. Rupp, *J. Mater. Chem. A* **2019**, *7*, 21299.

[9] a) J. van den Broek, S. Afyon, J. L. M. Rupp, *Adv. Energy Mater.* **2016**, *6*, 1600736; b) I. Garbayo, M. Struzik, W. J. Bowman, R. Pfenninger, E. Stilp, J. L. M. Rupp, *Adv. Energy Mater.* **2018**, *8*, 1702265.

[10] Z. Z. Zhang, Y. J. Shao, B. Lotsch, Y. S. Hu, H. Li, J. Janek, L. F. Nazar, C. W. Nan, J. Maier, M. Armand, L. Q. Chen, *Energy Environ. Sci.* **2018**, *11*, 1945.

[11] a) S. Wenzel, S. Randau, T. Leichtweiß, D. A. Weber, J. Sann, W. G. Zeier, J. Janek, *Chem. Mater.* **2016**, *28*, 2400; b) W. Zhang, F. H. Richter, S. P. Culver, T. Leichtweiss, J. G. Lozano, C. Dietrich, P. G. Bruce, W. G. Zeier, J. Janek, *ACS Appl. Mater. Interfaces* **2018**, *10*, 22226.

[12] Y. L. Song, L. Y. Yang, W. G. Zhao, Z. J. Wang, Y. Zhao, Z. Q. Wang, Q. H. Zhao, H. Liu, F. Pan, *Adv. Energy Mater.* **2019**, *9*, 1900671.

[13] T. Swamy, R. Park, B. W. Sheldon, D. Rettenwander, L. Porz, S. Berendts, R. Uecker, W. C. Carter, Y.-M. Chiang, *J. Electrochem. Soc.* **2018**, *165*, A3648.

[14] F. Han, A. S. Westover, J. Yue, X. Fan, F. Wang, M. Chi, D. N. Leonard, N. J. Dudney, H. Wang, C. Wang, *Nat. Energy* **2019**, *4*, 187.

[15] a) H. Buschmann, J. Dölle, S. Berendts, A. Kuhn, P. Bottke, M. Wilkening, P. Heitjans, A. Senyshyn, H. Ehrenberg, A. Lotnyk, V. Duppel, L. Kienle, J. Janek, *Phys. Chem. Chem. Phys.* **2011**, *13*, 19378; b) E. Rangasamy, J. Wolfenstine, J. Sakamoto, *Solid State Ionics* **2012**, *206*, 28; c) T. Thompson, S. Yu, L. Williams, R. D. Schmidt, R. Garcia-Mendez, J. Wolfenstine, J. L. Allen, E. Kioupakis, D. J. Siegel, J. Sakamoto, *ACS Energy Lett.* **2017**, *2*, 462; d) M. Yi, T. Liu, X. Wang, J. Li, C. Wang, Y. Mo, *Ceram. Int.* **2019**, *45*, 786.

[16] H. K. Tian, B. Xu, Y. Qi, *J. Power Sources* **2018**, *392*, 79.

[17] a) X. Guo, J. Fleig, J. Maier, *J. Electrochem. Soc.* **2001**, *148*, J50; b) M. J. Verkerk, B. J. Middelhuis, A. J. Burggraaf, *Solid State Ionics* **1982**, *6*, 159.

[18] R. Wagner, G. J. Redhammer, D. Rettenwander, A. Senyshyn, W. Schmidt, M. Wilkening, G. Amthauer, *Chem. Mater.* **2016**, *28*, 1861.

[19] a) I. Riess, *Solid State Ionics* **2003**, *157*, 1; b) I. Riess, *Solid State Ionics* **1992**, *51*, 219.

[20] a) R. Amin, P. Balaya, J. Maier, *Electrochem. Solid-State Lett.* **2007**, *10*, A13; b) S. Wang, M. Yan, Y. Li, C. Vinado, J. Yang, *J. Power Sources* **2018**, *393*, 75.

[21] a) J. Awaka, N. Kijima, H. Hayakawa, J. Akimoto, *J. Solid State Chem.* **2009**, *182*, 2046; b) A. Kuhn, S. Narayanan, L. Spencer, G. Goward, V. Thangadurai, M. Wilkening, *Phys. Rev. B* **2011**, *83*, 094302; c) G. Menzer, *Z. Kristallogr. - Cryst. Mater.* **1929**, *69*, 300.

[22] B. Stanje, D. Rettenwander, S. Breuer, M. Uitz, S. Berendts, M. Lerch, R. Uecker, G. Redhammer, I. Hanzu, M. Wilkening, *Ann. Phys.* **2017**, *529*, 1700140.

[23] a) N. Zhao, W. Khokhar, Z. J. Bi, C. Shi, X. X. Guo, L. Z. Fan, C. W. Nan, *Joule* **2019**, *3*, 1190; b) J. Su, X. Huang, Z. Song, T. Xiu, M. E. Badding, J. Jin, Z. Wen, *Ceram. Int.* **2019**, *45*, 14991; c) A. J. Samson, K. Hofstetter, S. Bag, V. Thangadurai, *Energy Environ. Sci.* **2019**, *12*, 2957.

[24] S. Qin, X. Zhu, Y. Jiang, M. e. Ling, Z. Hu, J. Zhu, *Appl. Phys. Lett.* **2018**, *112*, 113901.

[25] S. Emmert, M. Wolf, R. Gulich, S. Krohns, S. Kastner, P. Lunkenheimer, A. Loidl, *Eur. Phys. J. B* **2011**, *83*, 157.

[26] Y. Song, L. Yang, L. Tao, Q. Zhao, Z. Wang, Y. Cui, H. Liu, Y. Lin, F. Pan, *J. Mater. Chem. A* **2019**, *7*, 22898.

[27] a) I. Hanghofer, M. Brinek, S. L. Eisbacher, B. Bitschnau, M. Volck, V. Hennige, I. Hanzu, D. Rettenwander, H. M. R. Wilkening, *Phys. Chem. Chem. Phys.* **2019**, *21*, 8489; b) M. A. Kraft, S. P. Culver, M. Calderon, F. Bocher, T. Krauskopf, A. Senyshyn, C. Dietrich, A. Zevalkink, J. Janek, W. G. Zeier, *J. Am. Chem. Soc.* **2017**, *139*, 10909; c) I. Hanghofer, B. Gadermaier, H. M. R. Wilkening, *Chem. Mater.* **2019**, *31*, 4591.

[28] a) S. Lunghammer, D. Prutsch, S. Breuer, D. Rettenwander, I. Hanzu, Q. Ma, F. Tietz, H. M. R. Wilkening, *Sci. Rep.* **2018**, *8*, 11970; b) S. Lunghammer, Q. Ma, D. Rettenwander, I. Hanzu, F. Tietz, H. M. R. Wilkening, *Chem. Phys. Lett.* **2018**, *701*, 147.

[29] D. Di Stefano, A. Miglio, K. Robeyns, Y. Filinchuk, M. Lechartier, A. Senyshyn, H. Ishida, S. Spannenberger, D. Prutsch, S. Lunghammer, D. Rettenwander, M. Wilkening, B. Roling, Y. Kato, G. Hautier, *Chem* **2019**, *5*, 2450.

[30] N. Kamaya, K. Homma, Y. Yamakawa, M. Hirayama, R. Kanno, M. Yonemura, T. Kamiyama, Y. Kato, S. Hama, K. Kawamoto, A. Mitsui, *Nat. Mater.* **2011**, *10*, 682.

[31] L. Buannic, B. Orayech, J.-M. López Del Amo, J. Carrasco, N. A. Katcho, F. Aguesse, W. Manalastas, W. Zhang, J. Kilner, A. Llordés, *Chem. Mater.* **2017**, *29*, 1769.

[32] a) P. Posch, S. Lunghammer, S. Berendts, S. Ganschow, G. J. Redhammer, A. Wilkening, M. Lerch, B. Gadermaier, D. Rettenwander, H. M. R. Wilkening, *Energy Storage Mater.* **2020**, *24*, 220; b) P. J. Kumar, K. Nishimura, M. Senna, A. Düvel, P. Heitjans, T. Kawaguchi, N. Sakamoto, N. Wakiya, H. Suzuki, *RSC Adv.* **2016**, *6*, 62656.

[33] J. Zhao, B. Wang, K. Lu, *Ceram. Int.* **2014**, *40*, 14229.

[34] A. J. Samson, K. Hofstetter, E. Wachsman, V. Thangadurai, *J. Electrochem. Soc.* **2018**, *165*, A2303.

[35] J. Wolfenstine, J. Ratchford, E. Rangasamy, J. Sakamoto, J. L. Allen, *Mater. Chem. Phys.* **2012**, *134*, 571.

[36] M. Philipp, S. Lunghammer, I. Hanzu, M. Wilkening, *Mater. Res. Express* **2017**, *4*, 075508.

[37] M. Kubicek, A. Wachter-Welzl, D. Rettenwander, R. Wagner, S. Berendts, R. Uecker, G. Amthauer, H. Hutter, J. Fleig, *Chem. Mater.* **2017**, *29*, 7189.

[38] a) S. Smetaczek, M. Bonta, A. Wachter-Welzl, S. Taibl, R. Wagner, D. Rettenwander, J. Fleig, A. Limbeck, *J. Anal. At. Spectrom.* **2020**, *35*, 972; b) A. Wachter-Welzl, J. Kirowitz, R. Wagner, S. Smetaczek, G. C. Brunauer, M. Bonta, D. Rettenwander, S. Taibl, A. Limbeck, G. Amthauer, J. Fleig, *Solid State Ionics* **2018**, *319*, 203.

[39] Y. Zhu, J. G. Connell, S. Tepavcevic, P. Zapol, R. Garcia-Mendez, N. J. Taylor, J. Sakamoto, B. J. Ingram, L. A. Curtiss, J. W. Freeland, D. D. Fong, N. M. Markovic, *Adv. Energy Mater.* **2019**, *9*, 1803440.